Journal of Power Sources 190 (2009) 184–188

Contents lists available at ScienceDirect

Journal of Power Sources

journal homepage: www.elsevier.com/locate/jpowsour

Short communication

Modeling of the capacity loss of a 12 V automotive lead-acid battery due to ageing and comparison with measurement data

Ui Seong Kim[a], Chee Burm Shin[a,*], Seung Myun Chung[b], Sung Tae Kim[b], Byung Won Cho[c]

[a] Department of Chemical Engineering and Division of Energy Systems Research, Ajou University, Suwon 443-749, Republic of Korea
[b] Research & Development Division, Hyundai Motor Company, Whasung 445-706, Republic of Korea
[c] Battery Research Center, Korea Institute of Science and Technology, Seoul 136-791, Republic of Korea

ARTICLE INFO

Article history:
Received 9 June 2008
Received in revised form 21 December 2008
Accepted 22 December 2008
Available online 30 December 2008

Keywords:
Lead-acid battery
Ageing
Model
Finite element method

ABSTRACT

One-dimensional modeling was carried-out to predict the capacity loss of a 12 V automotive lead-acid battery due to ageing. The model not only accounted for electrochemical kinetics and ionic mass transfer in a battery cell, but also considered the anodic corrosion of lead in sulfuric acid. In order to validate the modeling, modeling results were compared with the measurement data of the cycling behaviors of the lead-acid batteries having nominal capacity of 68 Ah that are mounted on the automobiles manufactured by Hyundai Motor Company. The cycling was performed under the protocol of the constant-current discharge and the constant-voltage charge. The discharge rate of C/3 was used. The range of state of charge was between 1 and 0.85. The voltage was kept constant at the gassing voltage until the charge current tapered to 10 mA. The retention capacity of the battery was measured with C/3 discharge rate before the beginning of cycling and after every 40 cycles of cycling. The modeling results were in good agreement with the measurement data.

1. Introduction

The capacity of a lead-acid battery decreases with cycling due to the so-called ageing. The major ageing processes are known to be anodic corrosion, active mass degradation, irreversible formation of lead sulfate in the active mass, short-circuit and loss of water [1,2]. For the optimal design of the vehicle electric system, it is important to have a reliable modeling tool to quantify the ageing effects on the capacity loss of the automotive battery [3].

There have been many previous efforts on the ageing mechanisms and the expected lifetime of the lead-acid batteries. Lander elucidated the thermodynamics and kinetics of the corrosion process of lead in sulfuric acid in detail at potentials near the reversible $PbO_2/PbSO_4$ potential [4]. Ruetschi studied the influence of crystal structure and inter-particle contact on the capacity of PbO_2 electrode [5] and reviewed the ageing mechanisms and service life of lead-acid batteries [1]. Culpin and Rand reviewed the failure mechanisms of lead-acid batteries [6]. Armenta-Deu and Donaire investigated the kinetic aspects of the ageing factors for lead-acid batteries [7]. Nakamura et al. showed that the decline in the performance of valve-regulated lead-acid (VRLA) batteries is due not only to positive-plate degradation, but also to other causes that include negative-plate deterioration and poor separator-plate contact [8]. Cooper and Moseley reported the "premature capacity loss" (PCL) modes of the VRLA batteries. They referred a high resistance arising in the vicinity of the interface between the active material and the surface of the grid of the positive-plate as 'PCL-1,' a softening of the positive active mass as 'PCL-2,' and sulphation of the negative-plate in the case of high rate partial-state-of-charge duty as 'PCL-3' [9]. Wenzl et al. described the requirements for making lifetime predictions [10]. Sauer et al. presented several aspects of charging regimes and charge acceptance to reveal significant factors influencing lifetime and reliable battery operation [11]. Thele et al. proposed a model of the charge acceptance of lead-acid batteries including overcharging effects [12]. Schiffer et al. presented a comprehensive lifetime model of lead-acid batteries accounting for the impacts of operating conditions, system sizing and battery technology [2].

In this work, one-dimensional modeling was carried-out to predict the capacity loss of a 12 V automotive lead-acid battery due to ageing. The model accounted for the distributions of electrode and electrolyte potentials, electrochemical reaction rates, electrolyte concentration, and porosity in a battery cell, as well as the anodic corrosion of lead in sulfuric acid. In order to validate the modeling, modeling results were compared with the measurement data of the cycling behaviors of the lead-acid batteries having nominal capacity of 68 Ah that are mounted on the automobiles manufactured by Hyundai Motor Company.

* Corresponding author. Tel.: +82 31 219 2388; fax: +82 31 219 1612.
E-mail address: cbshin@ajou.ac.kr (C.B. Shin).

0378-7753/$ – see front matter © 2008 Elsevier B.V. All rights reserved.
doi:10.1016/j.jpowsour.2008.12.091

Nomenclature

a_1	volumetric change per mole of the material converted ($m^3\ mol^{-1}$)
a_2	coefficient accounting for volumetric ion production or consumption
A	specific active surface area of electrode (m^{-1})
c	acid concentration ($mol\ m^{-3}$)
c_{ref}	reference concentration ($mol\ m^{-3}$)
D^{eff}	effective diffusivity ($m^2\ s^{-1}$)
F	Faraday's constant (96,487 $C\ mol^{-1}$)
i_0	exchange current density ($A\ m^{-2}$)
j	transfer current density ($A\ m^{-3}$)
j_{corr}	corrosion rate ($A\ m^{-2}$)
j^0_{corr}	exchange current density of corrosion reaction ($A\ m^{-2}$)
j_{loss}	loss rate of active material ($A\ m^{-2}$)
k	electrical conductivity of corrosion layer ($A\ m^{-1}$)
k^{eff}	effective diffusion conductivity of the liquid phase ($A\ m^{-1}$)
k^{eff}_D	effective diffusion conductivity of the liquid phase due to diffusion ($A\ m^{-1}$)
M	molecular weight of corrosion product ($kg\ mol^{-1}$)
Q_{max}	theoretical electrode capacity ($C\ m^{-3}$)
R	universal gas constant ($8.3143\ J\ mol^{-1}\ K^{-1}$)
SOC	state of charge of electrodes
t	time (s)
T	absolute temperature (K)
U_{corr}	equilibrium potential of corrosion reaction (V)

Greek letters

α_a	anodic transfer coefficient
α_c	cathodic transfer coefficient
$\alpha_{c,corr}$	transfer coefficient of corrosion reaction
δ_f	film thickness (m)
ε	porosity of electrode
η	electrode overpotential (V)
η_{corr}	overpotential of corrosion reaction (V)
κ	electrolyte conductivity ($S\ m^{-1}$)
ρ	density ($kg\ m^{-3}$)
σ^{eff}	effective conductivity of the solid matrix ($S\ m^{-1}$)
ϕ	potential (V)

Subscripts

l	liquid phase
N	cycle number
s	solid phase

2. Mathematical model

A schematic diagram of the lead-acid cell is shown in Fig. 1. The cell is composed of a current collecting grid at the center of the negative electrode, a negative Pb electrode, a reservoir of electrolyte, a porous separator, a positive PbO_2 electrode, and a current collecting grid at the center of the positive electrode. In this work, the model considers the variations of the electrical potentials of the solid matrix of electrodes and the electrolyte, the acid concentration, the electrochemical kinetics, the state of charge of electrodes, and the electrode porosity. The governing equations expressing the above phenomena are listed in the following. The details of the model descriptions can be found in the references [13–15].(Conservation of charge in solid phase of electrode)

$$\nabla \cdot (\sigma^{eff} \nabla \phi_s) - Aj = 0 \quad (1)$$

(Conservation of charge in liquid phase of electrode)

$$\nabla \cdot (\kappa^{eff} \nabla \phi_l) + \nabla \cdot [\kappa^{eff}_D \nabla (\ln\ c)] + Aj = 0 \quad (2)$$

(Ionic species conservation)

$$\frac{\partial(\varepsilon c)}{\partial t} = \nabla \cdot (D^{eff} \nabla c) + a_2 \frac{Aj}{2F} \quad (3)$$

(Butler–Volmer equation for an electrochemical reaction)

$$j = i_0 \left(\frac{c}{c_{ref}}\right) \left[\exp\left(\frac{\alpha_a F}{RT}\eta\right) - \exp\left(-\frac{\alpha_c F}{RT}\eta\right)\right] \quad (4)$$

(Variation of SOC)

$$\frac{\partial(\mathrm{SOC})}{\partial t} = \pm \frac{\nabla \cdot i_l}{Q_{max}} \quad (5)$$

(Variation of porosity)

$$\frac{\partial \varepsilon}{\partial t} - a_1 \frac{Aj}{2F} = 0 \quad (6)$$

where ϕ_s is the potential of solid phase, ϕ_l is the potential of liquid phase, σ^{eff} is the effective conductivity of the solid matrix, A is the specific electroactive area, j is the transfer current density, κ^{eff} is the effective conductivity of the liquid phase, κ^{eff}_D is the effective conductivity of the liquid phase due to diffusion, c is the acid concentration, ε is the porosity, t is the time, D^{eff} is the effective diffusivity, a_2 is the coefficient accounting for volumetric ion production or consumption, F is the Faraday constant, i_0 is the exchange current density, c_{ref} is the reference concentration, α_a is the anodic transfer coefficient, α_c is the cathodic transfer coefficient, R is the universal gas constant, T is the absolute temperature, η is the electrode overpotential, SOC is the state of charge of electrodes, Q_{max} is the theoretical electrode capacity, a_1 is the volumetric change per mole of the material converted.

Although there are many processes associated with the ageing of lead-acid batteries as mentioned in the introduction, the model pre-

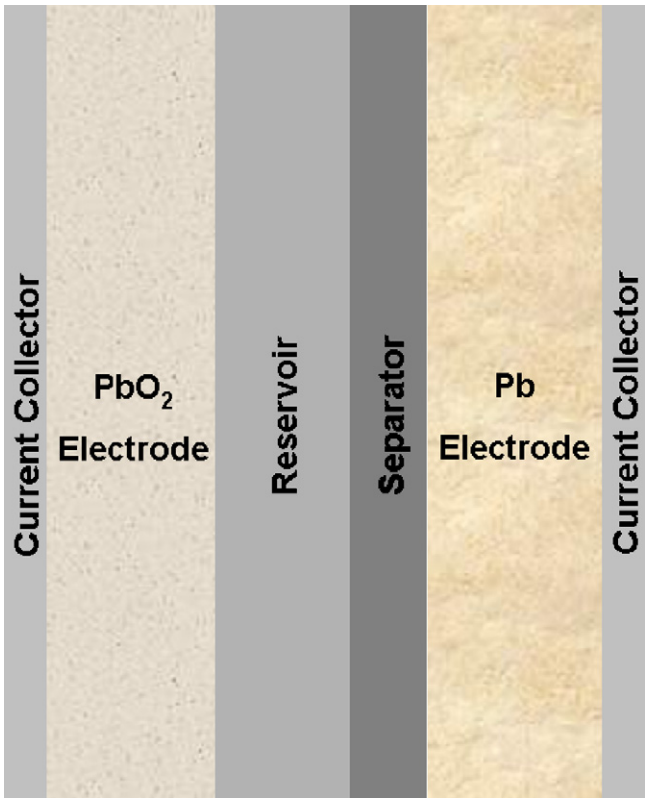

Fig. 1. Schematic diagram of a lead-acid cell.

sented in this work does not aim to include all processes which may cause the ageing of lead-acid batteries. The anodic corrosion of electrode and the loss of active material are the two ageing mechanisms that are considered in the model, because the automotive lead-acid batteries in passenger car used are usually ageing by anodic corrosion [1]. In order to accommodate corrosion, it is used as the concept of a corrosion layer with lower conductivity, which grows over the lifetime of the battery [2]. The corrosion layer thickness is given by

$$\frac{\partial \delta_f|_N}{\partial t} = -\frac{j_{corr}|_N \times M}{\rho F} \quad (7)$$

where $\delta_{f|N}$ is the film thickness after N cycles, $j_{corr|N}$ is the corrosion rate after N cycles, and M and ρ are the molecular weight and density of corrosion product, respectively. The corrosion rate is assumed to follow the anodic Tafel kinetics as

$$j_{corr} = -j^o_{corr} \exp\left(\frac{\alpha_{c,corr} F}{RT} \eta_{corr}\right) \quad (8)$$

$$\eta_{corr} = \phi_s - \phi_l - U_{corr} - jR_f \quad (9)$$

where j^o_{corr}, $\alpha_{c,corr}$, η_{corr}, and U_{corr} are the exchange current density, transfer coefficient, overpotential, and equilibrium potential of corrosion reaction, respectively. Electrical resistance of corrosion layer after N cycles, $R_{f|N}$, is related to the film thickness after N cycles by

$$R_f|_N = \frac{\delta_f|_N}{k} \quad (10)$$

where k is the electrical conductivity of corrosion layer. The loss rate of active material after N cycles is assumed to be proportional to the corrosion rate and the proportionality constant of this relation is treated as a fitting parameter to be determined by the comparison of the modeling results with the experimental data. Then, the electrode capacity loss is given by

$$Q_{loss} = \int_0^t A j_{loss} dt \quad (11)$$

where j_{loss} is the loss rate of active material. The electrode capacity after N cycles is updated by

$$Q_{N+1} = Q_N - Q_{loss}|_N \quad (12)$$

3. Results and discussion

The solutions to the governing equations subject to the associated boundary conditions were obtained by using the finite element method. In order to validate the modeling, modeling results were compared with the measurement data of the cycling behaviors of the lead-acid batteries having nominal capacity of 68 Ah that are mounted on the automobiles manufactured by Hyundai Motor Company. The cycling was performed under the protocol of the constant current (CC) discharge and the constant voltage (CV) charge at 75 °C. The discharge rate of C/3 was used. The charging voltage was kept constant at the gassing voltage until the charge current tapered to 10 mA. The range of state of charge during cycling was between 1 and 0.85. The retention capacity (RC) of the battery was measured with the discharge rate of C/3 until the voltage dropped to the cutoff voltage of 10.5 V at 25 °C before the beginning of cycling and after every 40 cycles of cycling. After the deep discharge to measure the RC, the battery was charged at 25 °C with the constant current of 50 A till the voltage reached the gassing voltage followed by CV charging until the charge current dropped to 10 mA. The discharge and charge procedures are illustrated schematically in Fig. 2.

Figs. 3 and 4 present the variation of the voltage and current of the battery during CC–CV charging after the RC measurements before the beginning of cycling and after 40 and 80 cycles. Modeling results and experimental measurements are in good agreement.

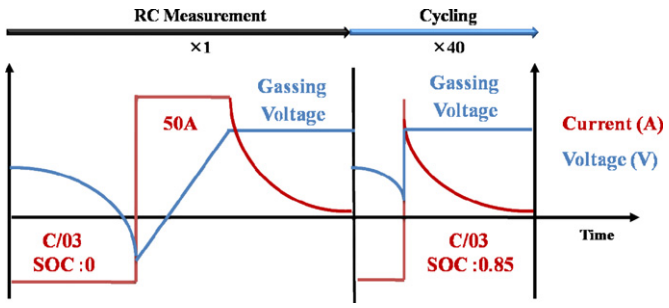

Fig. 2. Schematic illustration of the RC measurement and the cycling of a lead-acid battery.

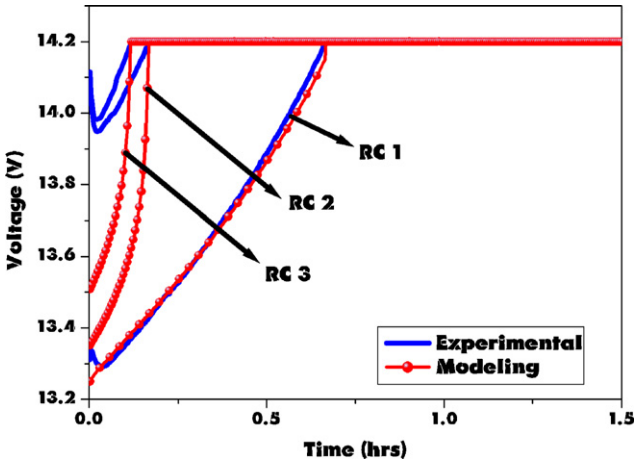

Fig. 3. Variation of voltage during CC–CV charging after the RC measurements.

As shown in Figs. 3 and 4, the model predicts a decrease in the CC charging time and increase of the CV charging time with the progress of cycling. The modeling results indicate that a gradual decrease in total charging time occurs with cycling. As a result of the corrosion, the electrical resistance of the corrosion layer continues to increase with cycling, which reduces the CC charging time due to continuous increase of voltage drop in the corrosion layer. Fig. 5 presents the charge curves that show the decrease in the capacity after the RC measurements. These include both CC and CV parts of the charging. Fig. 6 shows the discharge curves during the RC measurements. Due to the loss of active material, the SOC of the electrode material decreased while the capacity loss increased with

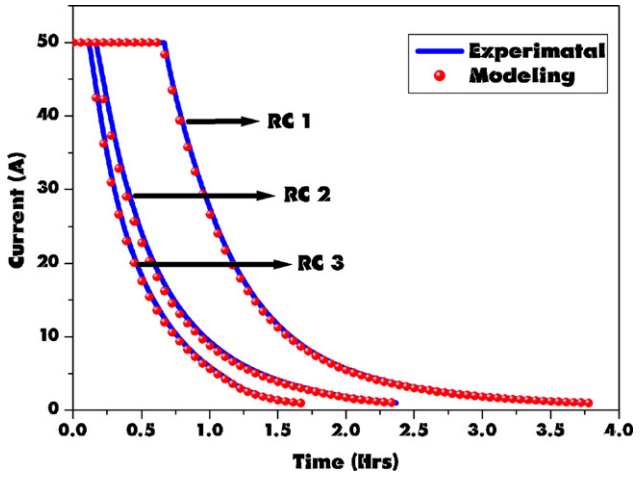

Fig. 4. Variation of current during CC–CV charging after the RC measurements.

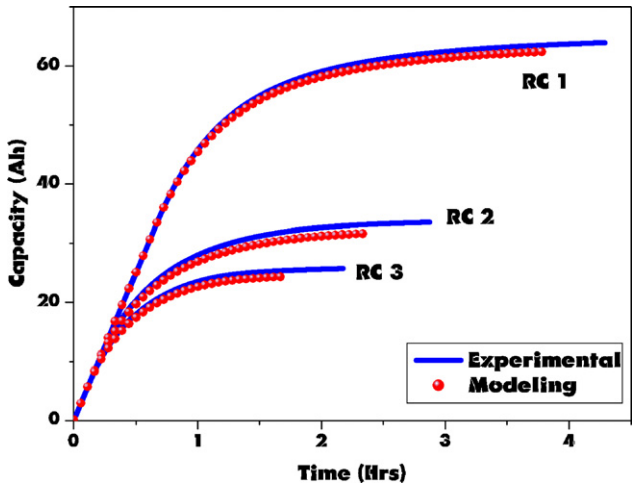

Fig. 5. Charge curves after the RC measurements.

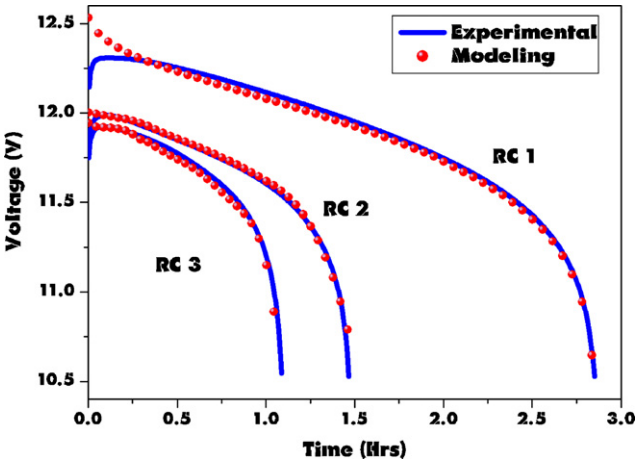

Fig. 6. Discharge curves during the RC measurements.

cycling. Apart from the capacity loss with continued cycling, the voltage plateau of discharge curves continued to decrease, which may be attributed to the continuous increase of the electrical resistance of the corrosion layer as a result of corrosion. The modeling results of Figs. 5 and 6 agree well with the measurement data.

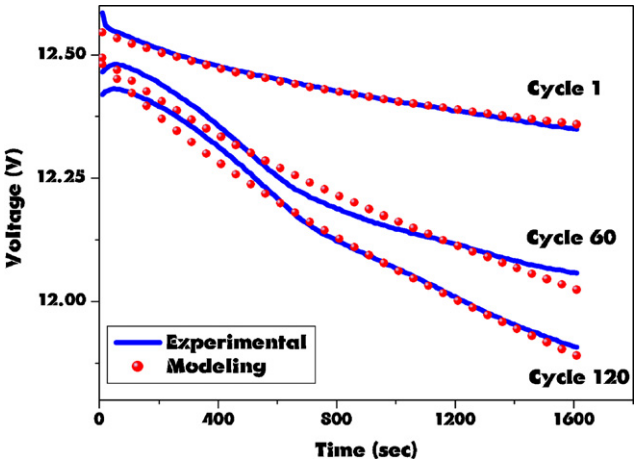

Fig. 7. Discharge curves during cycling at the range of SOC between 1 and 0.85 for various cycles.

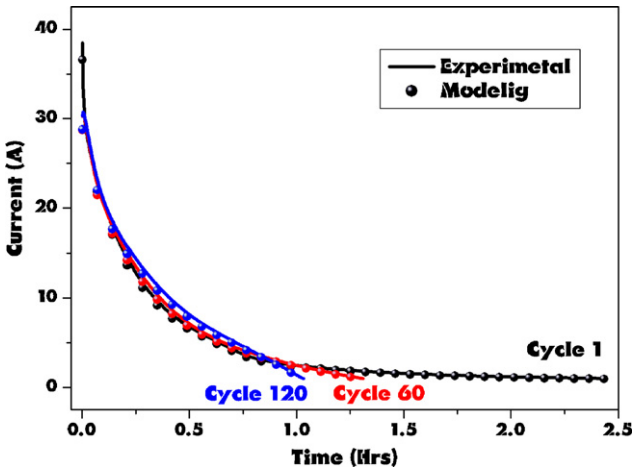

Fig. 8. Variation of current during the CV charging from the SOC value of 0.85 until the charge current drops to 10 mA for various cycles.

Discharge curves during cycling at the range of SOC between 1 and 0.85 are shown in Fig. 7. The voltage plateau decreased with cycling due to ageing. Fig. 8 shows the charging curves during the CV charging from the SOC value of 0.85 until the charge current drops to 10 mA. With the progress of cycling, the capacity loss of the battery was observed with cycling, which may be attributed to the combined effects of the gradual increase of corrosion layer and loss of active mass due to cycling and the detrimental stress imposed by the deep discharge of the RC measurements. Modeling results and experimental measurements are again in good agreement in Figs. 7 and 8.

4. Conclusions

A mathematical procedure was developed to study the ageing of a lead-acid battery. One-dimensional modeling was carried-out to predict the capacity loss of a 12 V automotive lead-acid battery due to ageing by using the finite element method. In order to validate the modeling, modeling results were compared with the measurement data of the cycling behaviors of the lead-acid batteries having nominal capacity of 68 Ah. Modeling results on the discharge and charge characteristics during cycling were in good agreement with the experimental measurements. The model predicted the capacity loss and the decrease of the voltage plateau of discharge curves with continued cycling, which may be attributed to the increase of the electrical resistance of the corrosion layer as a result of corrosion. The modeling methodology presented in this study may contribute to the optimal design of the battery management system of the vehicle.

Acknowledgements

This work was supported by NGV Corporation. One of the authors (C.B. Shin) acknowledges the Korea Science and Engineering Foundation (KOSEF R01-2006-000-10239-0) and the Ministry of Commerce, Industry and Energy of Republic of Korea (2007-E-1D25-P-02-0-00) for providing partial financial supports for this work.

References

[1] P. Ruetschi, J. Power Sources 127 (2004) 33–44.
[2] J. Schiffer, D.U. Sauer, H. Bindner, T. Cronin, P. Lundsager, R. Kaiser, J. Power Sources 168 (2007) 66–78.
[3] E. Meissner, G. Richter, J. Power Sources 144 (2005) 438–460.
[4] J.J. Lander, J. Electrochem. Soc. 103 (1956) 1–8.
[5] P. Ruetschi, J. Electrochem. Soc. 139 (1992) 1347–1351.

[6] B. Culpin, D.A.R. Rand, J. Power Sources 36 (1991) 415–438.
[7] C. Armenta-Deu, T. Donaire, J. Power Sources 58 (1996) 123–133.
[8] K. Nakamura, M. Shiomi, K. Takahashi, M. Tsubota, J. Power Sources 59 (1996) 153–157.
[9] A. Cooper, P.T. Moseley, J. Power Sources 113 (2003) 200–208.
[10] H. Wenzl, I. Baring-Gould, R. Kaiser, B.Y. Liaw, P. Lundsager, J. Manwell, A. Ruddell, V. Svoboda, J. Power Sources 144 (2005) 373–384.
[11] D.U. Sauer, E. Karden, B. Fricke, H. Blanke, M. Thele, O. Bohlen, J. Schiffer, J.B. Gerschler, R. Kaiser, J. Power Sources 168 (2007) 22–30.
[12] M. Thele, J. Schiffer, E. Karden, E. Surewaard, D.U. Sauer, J. Power Sources 168 (2007) 31–39.
[13] H. Gu, T.V. Nguyen, R.E. White, J. Electrochem. Soc. 134 (1987) 2953–2960.
[14] D.M. Bernardi, H. Gu, A.Y. Schoene, J. Electrochem. Soc. 140 (1993) 2250–2258.
[15] W.B. Gu, C.Y. Wang, B.Y. Liaw, J. Electrochem. Soc. 144 (1997) 2053–2061.